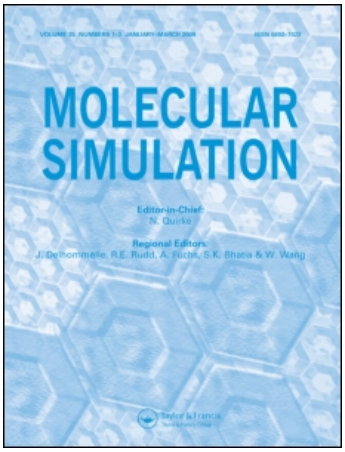

Molecular Simulation
Publication details, including instructions for authors and subscription information:
http://www.informaworld.com/smpp/title~content=t713644482

The anticancer drug bleomycin investigated by density functional theory

A. Karawajczyk[a]; F. Buda[a]
[a] Leiden Institute of Chemistry, Leiden University, Leiden, RA, The Netherlands

To cite this Article Karawajczyk, A. and Buda, F.(2006) 'The anticancer drug bleomycin investigated by density functional theory', Molecular Simulation, 32: 15, 1233 — 1239
To link to this Article: DOI: 10.1080/08927020601101083
URL: http://dx.doi.org/10.1080/08927020601101083

Molecular Simulation, Vol. 32, No. 15, 30 December 2006, 1233–1239

Taylor & Francis
Taylor & Francis Group

The anticancer drug bleomycin investigated by density functional theory

A. KARAWAJCZYK and F. BUDA*

Leiden Institute of Chemistry, Leiden University, PO Box 9502, 2300 RA, Leiden, The Netherlands

(Received June 2006; in final form November 2006)

Activated bleomycin (ABLM) is an oxygenated iron drug complex which embodies the drug's DNA-cleaving activity. This activity is exercised on DNA, if present, but if DNA is absent, the drug itself is inactivated. We have employed quantum density functional theory (DFT)-based methods to investigate (i) the structure of the Fe(II)BLM complex that is first formed in the human body after drug's administration, and (ii) the activation mechanism of the O—O bond present in the ABLM. We have identified the controversial second axial ligand as the endogenous oxygen atom of the carbamoyl group. Our first principles molecular dynamics (MD) simulations indicate a homolytic cleavage as the mechanism of the O—O bond activation in the ABLM complex.

Keywords: Bleomycin; O—O bond activation; Density functional theory; Car–Parrinello molecular dynamics simulations; Iron–oxo complex

1. Introduction

Bleomycin (BLM) is a drug commonly used in chemotherapy since the early 80s against several types of cancer, including cervix and uterus cancer, head and neck cancer, testicle and penile cancer and certain types of lymphoma [1]. The precise mechanism(s) of action of BLM is not fully known. The drug in metal free form is administrated to patients. In the body, it forms the Fe(II)BLM complex with an iron atom and then binds O_2 to generate the O_2—Fe(II)—BLM complex. This complex is converted into activated bleomycin (ABLM) (BLM—Fe(III)—OOH) [2–5] and then is bound to DNA. BLM kills cells by binding and then degrading genetic material (DNA) by cutting a strand of DNA. It carries out this process in the dividing phase of the cell's life cycle and so prevents the cell from growing. Unfortunately, BLM also affects the healthy cells causing so-called side effects. The most dangerous side effect, which is fatal lung fibrosis, is probably related to the high reactivity of the activated BLM with an iron as the metal cofactor. The BLM—Fe(III)—OOH complex has a half-life time at 6°C and pH = 7.0 equal to 6 min [3] and it can undergo self-inactivation or can react with DNA, if present, causing its degradation [3]. The first step of the reaction, which involves the activation of the O—O bond is not known. In the past, the hypothesis of heterolytic cleavage was proposed based on the similarity to the cytochrome P450 [1,6,7]. Recently, this idea has been reviewed and homolytic activation is also pointed out as a possible mechanism [8,9]. Thus in this work, we have addressed the following unknown or unclear issues for the anticancer antibiotic BLM:

(i) First we investigated the geometry of the Fe(II)BLM complex in vacuum. The exact coordination of the ligand has been a matter of dispute for several years. Specifically, the exact nature of the second axial ligand has been questioned, being identified either with an oxygen atom or a nitrogen atom of the carbamoyl group. Most of the knowledge available on the structure of various metallo-BLM complexes in solution is derived from spectroscopic data [10,11] and studies combining multinuclear NMR experiments and molecular dynamics (MD) simulations [12,13]. Some advanced computational methods were also applied but on simplified models which introduce some uncertainty [14].

(ii) Next we focused on the mechanism of the O—O bond activation in the ABLM complex. First

*Corresponding author. Email: f.buda@chem.leidenuniv.nl

Molecular Simulation
ISSN 0892-7022 print/ISSN 1029-0435 online © 2006 Taylor & Francis
http://www.tandf.co.uk/journals
DOI: 10.1080/08927020601101083

principles MD simulations were performed to follow the first reaction step in BLM self-inactivation in water solution in the absence of DNA. From experimental results it is known that ABLM may decay in the absence of DNA and an irreversible change in BLM occurs. It undergoes a conversion to one or more Fe(III) complexes unable to attack DNA even when aerobic Fe(II) is subsequently added [15]. The reaction is called ABLM suicide because ABLM is a kinetic component in this reaction [3]. The suicide chemistry is very complex [16], yielding several products [4] and likely involving a modification of the bithiazole moiety [17] but still the exact mechanism is under discussion. Our computational method allows studying the reaction without the need of a predefined reaction path.

(iii) Finally, we have addressed the reaction mechanism of ABLM with a deoxyribose sugar in vacuum. It is known from experiment that the degradation of DNA starts by forming a radical at C′4 position of a deoxyribose sugar [1]. Once again, the mechanism of the radical formation is not known.

This paper shows that quantum mechanics based computational tools may be essential to investigate the chemical activity of drugs. Since the size of the systems involved is quite large (often thousands of atoms) we need to combine methods with different accuracy and computational cost. Specifically, hybrid quantum mechanics–molecular mechanics (QM/MM) approaches are particularly promising in addressing these issues.

2. Models and computational methods

The models used in our study are based on the NMR data for a BLM—Co(III)—OOH complex bonded to a fragment of DNA (D(GGAAGCTTCC)) [18]. The structure is presented in figure 1. In the BLM ligand, we can distinguish three main parts: the metal bonding domain, the sugar moiety and the bithiazole tail. While the sugar moiety and the bithiazole tail are responsible for recognition and docking to DNA, the metal bonding domain plays a main role in the metal coordination and the O—O bond activation. Therefore for studying the reaction mechanisms, we have chosen the metal bonding domain (represented in stick and balls in figure 1) to be described by quantum methods without further simplifications. The equatorial ligands are: the secondary amine of the β-aminoalanine (A″aALA—N2) segment, the pyrimidine (PYR—N3), the imidazole ring (HIS-I—N5) and the amide nitrogen (HIS-A—N4) of the β-hydroxyhistidine. The primary amine of the β-aminoalanine residue (A′aALA—N1) and the oxygen atom of the peroxy group are the two axial ligands.

The deoxyribose sugar (indicated in cyan in figure 1) was included into the model to study the reaction of ABLM with the sugar in the position taken from the presented structure. The positions of the oxygen atoms

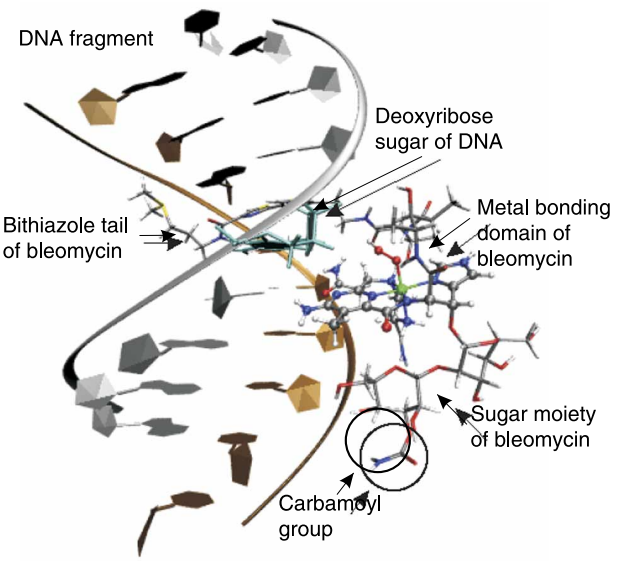

Figure 1. The NMR structure of BLM—Co(III)—OOH bound to the fragment of DNA (D(GGAAGCTTCC)) [18]. The structure of the BLM complex is represented in color following standard atomic color definition. The three parts of BLM are indicated: (i) the bithiazole tail that is inserted between two pairs of DNA; (ii) the metal bonding domain represented in stick and balls that is treated quantum-mechanically in the present work; (iii) the sugar moiety with the carbamoyl group. The deoxyribose sugar of DNA, indicated in cyan in the figure, is the one attacked by ABLM in the first step of DNA degradation.

bonded originally to phosphor were fixed during the simulations.

The sugar moiety of the BLM appears to be important in the structure determination of the Fe(II)—BLM complex and therefore it has been included in the quantum description. We have constructed two models: one with an oxygen atom (complex **A**) from the carbamoyl group of the sugar bonded to the iron center in the axial position and the second with a nitrogen atom (complex **B**) bonded to the iron center. The aim of these calculations was to identify the second axial ligand and compare the results with available experimental data.

To solve the structure of the Fe(II)—BLM complex, we have performed density functional theory (DFT) calculations using the B3LYP functional, which was shown to predict the correct spin ground state for a number of different iron complexes [19]. We used the effective core potential basis set LanL2DZ [20] for the iron atom and the 6-31G basis set for the other atoms as implemented in the program GAUSSIAN98 [21]. The LanL2DZ basis set was examined by Solomon *et al.* for ABLM [8] and it was shown to be good enough to describe the geometry of ABLM. The results obtained with a triple-ζ all electron basis set give a comparable description.

To investigate the reaction mechanisms, we used the Car–Parrinello molecular dynamics (CPMD) method [22] as implemented in the CPMD code [23]. The Kohn–Sham orbitals are expanded in a plane wave (PW) basis set with a kinetic energy cutoff of 80 Ry. We employed Martins-Troullier *ab initio* norm-conserving pseudopotentials [24]. Our test calculations proved that the energy cutoff of 80 Ry

is sufficient for achieving a good convergence of energies and structural properties for the considered systems. We used a generalized gradient approximation for the exchange-correlation functional, following the prescription of Becke and Perdew (BP) [25,26]. All simulations are spin polarized with a total spin $S = 1/2$. Room temperature CPMD simulations were performed by using a time step of 0.09 fs and a value of 400 a.u. for the fictitious electronic mass in the Car–Parrinello Lagrangian.

For the simulation including the sugar in vacuum, we have used an isolated cubic supercell of size $18 \times 18 \times 18$ Å^3. The simulation in water was performed using a hybrid QM/MM approach [27,28]. In particular, the hybrid QM/MM scheme used here is based on the CPMD method for the quantum part and on the Gromos96 MD program [29] for the classical molecular mechanics part. The quantum mechanics part includes the model of ABLM and six water molecules in a cubic box of $15 \times 15 \times 15$ Å^3. The rest of the water molecules were described using the SPC model [30] with the force field implemented in the Gromos96 program.

3. Structure determination of the Fe(II)—BLM complex

The structure determination of proteins or other biomolecules is mostly done by molecular mechanics calculations using very reliable force fields. In the case of BLM, the presence of the transition metal introduces some difficulties in producing reliable force field parameters. Therefore, we have decided to use DFT static calculations to gain an insight in the coordination sphere of the complex by treating explicitly the electronic structure and the proper spin distribution of the complex.

For both systems under consideration (see figure 2) full geometry optimizations assuming low, intermediate and high spin state have been carried out. The final geometric parameters and electronic energies corresponding to singlet, triplet and quintet states are summarized in table 1. Complex **A** was found to have the lowest energy in its quintet electronic state and this energy is taken as the reference energy for other spin states of complexes **A** and **B**. Our investigation shows that the geometry of the drug complex is highly dependent on the environment of the iron ion and on its spin state. For complexes **A** and **B**, the distances between the iron metal and axial ligand change as a function of the spin state. For complex **A**, the Fe—$O_{carbamoyl}$ distance reaches a maximum value for $S = 1$ (see table 1) equal to 3.26 Å indicating that the bond is broken. For $S = 2$, the Fe—$O_{carbamoyl}$ bond is again present with a length of 2.29 Å. For complex **B**, the Fe—$N_{carbamoyl}$ bond increases consistently up to 4.02 Å for $S = 2$.

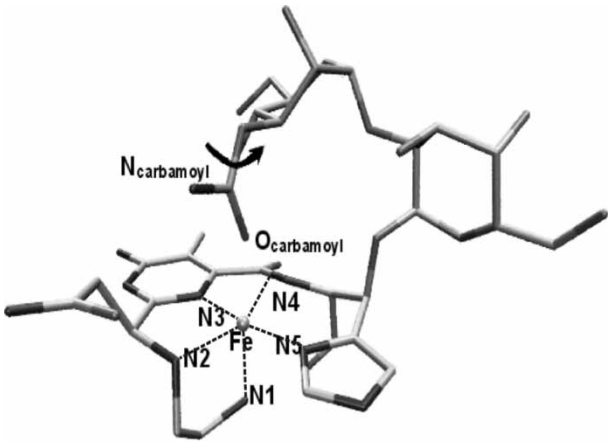

Figure 2. Model of the metal coordination domain of Fe(II)BLM with two different axial ligands: (i) the oxygen atom from the carbamoyl group (complex **A**) and (ii) the nitrogen atom from carbamoyl group (complex **B**). Complex **B** was created by rotating the carbamoyl group via the torsion angle pointed out in the picture.

We also observe a large change in the valence angle of $O_{carbamoyl}$—Fe—N1 and a big distortion from planarity around the metal center for different spin states (table 1). For complex **A**, the angle changes from 170.3° for $S = 0$ to 140.8° for $S = 2$ while the largest distortion is observed for the complex **A** in its quintet ground state, with a dihedral angle N2—N3—N4—N5 of 14.7°. The angle distortion together with the distortion from planarity discussed above brings the complex into a highly distorted tetragonal geometry. Because of these modifications, the Fe—$O_{carbamoyl}$ bond becomes weaker and more susceptible to exchange with an oxygen molecule to produce the

Table 1. Relative energies (in kcal/mol) and optimized geometrical parameters of complexes **A**, **B** (see also figure 2).

	Complex A			*Complex B*		
Total spin	*0*	*1*	*2*	*0*	*1*	*2*
ΔE (kcal/mol)†	12.29	6.96	0.0	32.83	26.10	23.78
Fe–X‡	2.17	3.26	2.29	2.29	3.93	4.02
Fe—N1	2.03	2.26	2.22	2.04	2.27	2.19
Fe—N2	2.16	2.13	2.40	2.14	2.15	2.30
Fe—N3	1.92	1.92	2.13	1.90	1.91	2.07
Fe—N4	1.97	1.94	2.09	1.98	1.94	2.03
Fe—N5	2.01	2.03	2.22	2.01	2.03	2.18
X—Fe—N1	170.3	126.2	140.8	176.8	168.4	166.2
2–3–4–5	7.0	9.4	14.7	5.9	7.0	9.4

All distances are in Å and angles in degrees. The last row refers to the dihedral angle formed by the equatorial N ligands (see also figure 2).
† For complexes **A** and **B**, the reference energy is the ground quintet electronic state energy of the complex **A**, which has the value $E_{ref} = -2968.6627$ a.u.
‡ X=$O_{carbamoyl}$, $N_{carbamoyl}$ for complex **A**, **B**, respectively.

BLM—Fe(II)—O_2 complex. This complex then accepts an additional electron to form the activated BLM species. Previous studies for Co—BLM based on force field methods [31,32], have proposed six-coordinate geometries with either five or six endogenous ligands. The crystal structure for copper–BLM [33] and some NMR studies for other metallo-BLM [18] are in agreement with our results. We have also calculated the root mean square deviation (RMSD) between experimental iron–proton distances obtained from relaxation times of the paramagnetically behaved protons [13] and our theoretical data. Once again the best fit to those values is given by complex **A** with a RMSD equal to 0.5 Å [34]. Our results strongly support the picture in which the atoms N1, N2, N3, N4, N5 remain in the coordination sphere of the metal center and the flexible sugar moiety drifts away making space for an exogenous ligand.

4. ABLM in H_2O

We now investigate the reaction mechanism of the ABLM self-inactivation in water [35]. This simulation will enable us to check the activation mechanism of the O—O bond in presence of the water solvent. To prepare the initial configuration of ABLM in water, we have performed a classical MD simulation using the Gromos96 program, in which the coordinates of the solute molecule were fixed while the 308 water molecules in the box have been relaxed. First, a constant pressure simulation at 300 K and 1 bar was performed for 2 ns and then a constant volume simulation was performed for 1 ns. After relaxation of the solvent molecules, six waters were found within a distance of 3 Å from the —OOH ligand and have been chosen to be present in the quantum part of the system. After the relaxation procedure, we have followed the trajectory for about 1 ps. We have illustrated the simulation in figure 3, where the Fe—O1, O1—O2, and O2—H_{W1} distances are plotted. During the first 500 fs, a network of the hydrogen bonds of the six quantum waters is formed. In this simulation, we observed the formation of an H-bond (after about 500 fs) between the OOH ligand and one of the water molecules (O2—H_{W1}). Simultaneously with the formation of this H-bond, the O1—O2 distance starts increasing (see figure 3, dotted line at 500 fs). Eventually, the O—O bond is broken but the released OH species remains H-bonded to the W1 water. After about 350 fs from the formation of the H-bond, the OH species forms a water molecule by abstracting a hydrogen atom from the W1 water molecule (see figure 3, dashed line at ∼850 fs). Next, we could observe a fast cascade of hydrogen atom abstraction where the OH species diffuses through the existing H-bond network of the water molecules.

To characterize the OH species, we performed a single point calculation for the configuration at 650 fs. The OH species was characterized as a hydroxyl radical with the spin density localized on the oxygen atom and with a small negative charge. For a complete picture of the observed reaction mechanism and identification of the products, we have also performed a single point calculation for the same configuration of the system at $t = 650$ fs but with a total spin of 3/2. The total energy was about 10 kcal/mol higher than for the system with total spin equal to 1/2. This result shows that no spin flip takes place and our implicit assumption about the conservation of the total spin during the reaction (shown below) was correct:

$$[Fe^{III}(BLM)—OOH]^+ \rightarrow [Fe^{IV}(BLM)=O]^+ + OH^{\cdot}$$
$$\uparrow \qquad\qquad \uparrow\uparrow \qquad\qquad \downarrow$$

In both single point calculations with different total spin, we observed the spin density localized mostly on the iron atom, the oxygen atom of the complex and on the oxygen atom of the OH species. The only difference is that the spin localized on the OH radical is a minority (β) spin for $S = 1/2$ while is a majority (α) spin for $S = 3/2$. We do not see any significant spin density on the equatorial ligands of the iron center thus ruling out the presence of cytochrome P450 compound I-like [BLM—Fe(V)=O]$^+$ complex. Importantly, this high-valent species, like

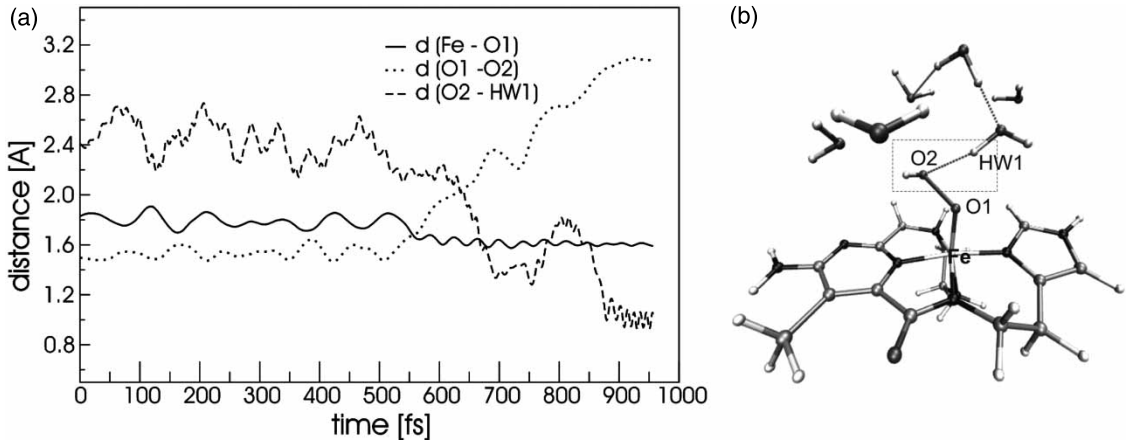

Figure 3. (a) Dynamic evolution of a few selected distances along the MD of ABLM in water: (i)– full line, Fe—O1; (ii) – – – dashed line, O2—H_{W1}; (iii)... dotted line, O1—O2. H_{W1} is the hydrogen atom from one of the water molecules included in the QM part which takes part in the formation of the hydrogen bond. (b) The structure of our ABLM model with six water molecules present in the QM part (the water molecules described by molecular mechanics are omitted for clarity). The hydrogen bond between O2 and H_{W1} is clearly visible in this snapshot.

cytochrome P450 compound I, is better described as an Fe(IV)═O unit magnetically coupled to a ligand radical with the ligand hole essentially localized on the deprotonated amide. A detailed study of the electronic structure of this Fe(V) compound was performed by static DFT calculation in Ref. [9].

5. ABLM with sugar

We have performed CPMD simulations to get an insight into the reaction of ABLM with the deoxyribose sugar which is attacked in the first step of the DNA degradation. In these simulations, we have included the ABLM complex and the sugar molecule in vacuum with all the atoms being treated quantum-mechanically with DFT using CPMD. We have increased slowly the temperature to 300 K and then followed the simulations for 1 ps. The sugar molecule has three hydrogen atoms available for abstraction (1′H, 2′H, 4′H). During the simulations, we observe the formation of H-bonds between the O2 atom of the —OOH group and all these hydrogens at different time intervals (see figure 4). We notice however that only the formation of a H-bond with 4′H has an influence on the amplitude of the O1—O2 bond length oscillation. In figure 4, we can see that when the O2—1′H and O2—2′H distances are shorter than O2—4′H, the O1—O2 bond remains stable oscillating with a small amplitude around the average value 1.5 Å. After 750 fs, the O2—4′H distance becomes the shortest one and immediately the O1—O2 bond distance starts increasing. After further 300 fs, the O1—O2 bond is broken and the water molecule H—O2—4′H is formed by direct hydrogen atom abstraction. The Fe—O distance drops from an average value of 1.8 to 1.65 Å indicating the formation of a stronger Fe═O double bond. The selectivity of the observed reaction is very interesting. The simulations show clearly the preference of H-bond formation with 4′H atom which is known to be abstracted in the reaction with DNA.

We decided to check the stability of three possible radicals of the deoxyribose sugar. We have noticed that the most stable radical is indeed the 4′C radical, which is lower in energy by 2.9 and 8.4 kcal/mol than 1′C and 2′C radicals, respectively. This result could explain the observed selectivity during our simulations. On the other hand, in the natural system the 1′C atom is connected to the cytosine. We have calculated the energy of the radicals 1′C and 4′C for a deoxycytidine and we have found that the presence of the aromatic ring in that position makes the 1′C radical most stable. However, the difference in energy is quite small, the 4′C radical being only 0.9 kcal/mol higher than the 1′C. In this situation other factors, such as steric and electrostatic interactions or the geometry of the formed H-bond, could change the relative stability of the radicals.

Our simulations show that the reaction mechanism of the O—O bond cleavage is very similar to the one observed in ABLM self-inactivation. In both cases, the H-bond is created before the scission takes place. We find that the BLM ligand with iron center facilitates a homolytic activation of the O—O bond. Although our simulations show a selective reaction in agreement with experimental indications, only explicit inclusion of the DNA environment can provide a stronger explanation for the selectivity of the H-abstraction reaction.

6. Conclusions

In this paper, we have presented DFT calculations and CPMD simulations to investigate structural properties and chemical activity of the anticancer drug BLM. The standard procedure in theoretical development and testing of new medicines is based mostly on statistical approaches like chemometrics or molecular mechanics calculations. While these methods are very helpful and successful in this field, they need to be supported by quantum-chemistry tools, particularly when dealing with chemical reactions. Specifically, DFT-based methods used in the present work appear to be appropriate for this aim.

Based on our results, we conclude that the second axial ligand of the Fe(II)—BLM complex is an oxygen atom

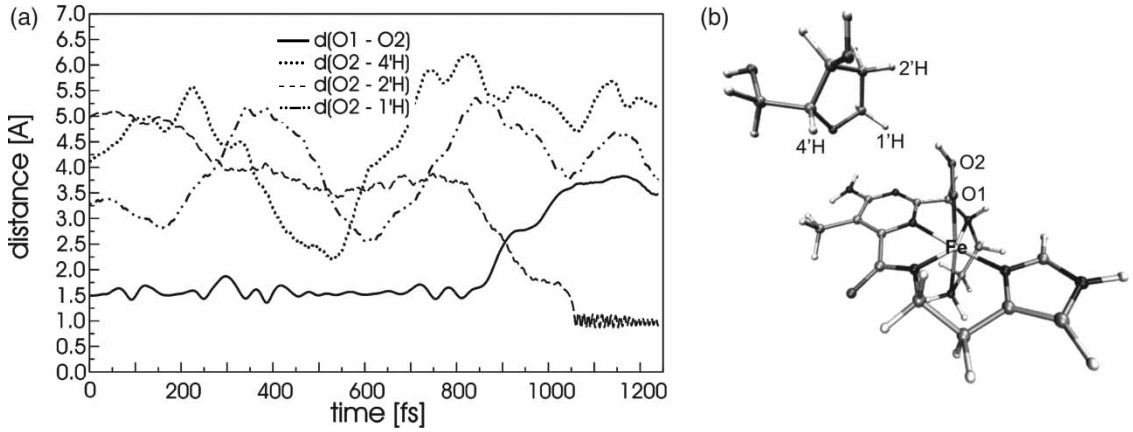

Figure 4. (a) Dynamic evolution of a few distances along the MD simulation of ABLM with the deoxyribose sugar: (i)– full line, O1—O2; (ii) – – – dotted line, O2—2′H; (iii) … dashed line, O2—4′H; and (iv) …… dot-dashed line, O2—1′H. (b) The structure of ABLM and the deoxyribose sugar model used in the simulations.

coming from the carbamoyl group of the sugar moiety. The optimized geometry of the complex is consistent with the parameters derived from NMR experiment [13] and moreover provides an indication on how the exchange with another external ligand like an oxygen molecule may occur. Interestingly, the geometries of complexes **A** and **B** are very similar for the lowest spin state $S = 0$, both having a six-fold coordination shell. We see major changes in the coordination shell only for the high spin state ($S = 2$, the experimentally observed one). This strong dependence of the final geometry on the electronic configuration makes a proper description in terms of force field modeling very complicated.

First principles MD simulations strongly support a homolytic cleavage as the mechanism of the O—O bond activation in ABLM complex. The reaction with sugar can be better characterized as a direct hydrogen atom abstraction. The just formed hydroxyl radical is hydrogen bonded with the 4′H of the sugar that is then abstracted to form a sugar radical and a water molecule. Thus, we can conclude that the selectivity of the observed homolytic O—O bond activation derives from the fact that the hydrogen bond is formed prior the bond scission and the hydroxyl radical is somehow trapped by a specific hydrogen bond.

The observed mechanism of the O—O bond cleavage of ABLM in water brings us to the same conclusions. Moreover, we think that the homolytic activation of that bond can be responsible for the self-degradation of ABLM. The hydroxyl radical can easily react with other parts of the ligand causing, for example, the experimentally observed modification of the bithiazole tail.

The results presented in this paper give a strong indication that in order to solve the issues related to the BLM complex, it is very important to have a realistic description of the system. On the other hand, it is not possible to study reaction mechanisms without a good quantum description of the electronic structure of the model. This implies some constraints on the size of the model. Therefore, we have to compromise on the level of accuracy by using a QM/MM approach. The next step in our ongoing research is to perform QM/MM simulations on a model of the BLM—Fe(III)—OOH complex bonded to DNA based on the NMR structure of the cobalt BLM complex [18]. In the first phase of our study, only the metal bonding domain with the iron center and the peroxy group is described by quantum methods (DFT). Our preliminary results confirm the experimentally observed protective role of DNA in the process of the ABLM self-inactivation [3]. A full account of QM/MM simulations including a DNA fragment will be presented elsewhere.

Acknowledgements

We thank Prof. U. Roethlisberger and members of her group at EPFL for providing and introducing us to the QM/MM hybrid code. We acknowledge the CYTTRON consortium for partially financing this project. The use of supercomputer facilities was sponsored by the Stichting Nationale Computer Faciliteiten (NCF), with financial support from Nederlandse Organisatie voor Wetenschappelijk Onderzoek (NWO).

References

[1] R.M. Burger. Cleavage of nucleic acids by bleomycin. *Chem. Rev.*, **98**, 1153 (1998).
[2] R.M. Burger, T.A. Kent, S.B. Horwitz, E. Munck, J. Peisach. Mossbauer study of iron bleomycin and its activation intermediates. *J. Biol. Chem.*, **258**, 1559 (1983).
[3] R.M. Burger, J. Peisach, S.B. Horwitz. Activated bleomycin—a transient complex of drug, iron, and oxygen that degrades DNA. *J. Biol. Chem.*, **256**, 1636 (1981).
[4] J.W. Sam, X.J. Tang, J. Peisach. Electrospray mass-spectrometry of iron bleomycin—demonstration that activated bleomycin is a ferric peroxide complex. *J. Am. Chem. Soc.*, **116**, 5250 (1994).
[5] T.E. Westre, K.E. Loeb, J.M. Zaleski, B. Hedman, K.O. Hodgson, E.I. Solomon. Determination of the geometric and electronic-structure of activated bleomycin using X-ray-absorption spectroscopy. *J. Am. Chem. Soc.*, **117**, 1309 (1995).
[6] M.R. Bukowski, S.R. Zhu, K.D. Koehntop, W.W. Brennessel, L. Que. Characterization of an Fe-III—OOH species and its decomposition product in a bleomycin model system. *J. Biol. Inorg. Chem.*, **9**, 39 (2004).
[7] T. Owa, T. Sugiyama, M. Otsuka, M. Ohno, K. Maeda. Synthetic studies on antitumor antibiotic bleomycin.30. A model study on the mechanism of the autoxidation of bleomycin. *Tetrahedron Lett.*, **31**, 6063 (1990).
[8] N. Lehnert, F. Neese, R.Y.N. Ho, L. Que, E.I. Solomon. Electronic structure and reactivity of low-spin Fe(III)–hydroperoxo complexes: comparison to activated bleomycin. *J. Am. Chem. Soc.*, **124**, 10810 (2002).
[9] F. Neese, J.M. Zaleski, K.L. Zaleski, E.I. Solomon. Electronic structure of activated bleomycin: oxygen intermediates in heme versus non-heme iron. *J. Am. Chem. Soc.*, **122**, 11703 (2000).
[10] K.E. Loeb, J.M. Zaleski, C.D. Hess, S.M. Hecht, E.I. Solomon. Spectroscopic investigation of the metal ligation and reactivity of the ferrous active sites of bleomycin and bleomycin derivatives. *J. Am. Chem. Soc.*, **120**, 1249 (1998).
[11] K.E. Loeb, J.M. Zaleski, T.E. Westre, R.J. Guajardo, P.K. Mascharak, B. Hedman, K.O. Hodgson, E.I. Solomon. Spectroscopic definition of the geometric and electronic-structure of the nonheme iron active-site in iron(II) bleomycin—correlation with oxygen reactivity. *J. Am. Chem. Soc.*, **117**, 4545 (1995).
[12] T.E. Lehmann. Molecular modeling of the three-dimensional structure of Fe(II)–bleomycin: are the Co(II) and Fe(II) adducts isostructural? *J. Biol. Inorg. Chem.*, **7**, 305 (2002).
[13] T.E. Lehmann, L.J. Ming, M.E. Rosen, L. Que. NMR studies of the paramagnetic complex Fe(II)–bleomycin. *Biochemistry*, **36**, 2807 (1997).
[14] M. Freindorf, P.M. Kozlowski. DFT study of the metal coordination center domain of Fe(II)–bleomycin. *J. Phys. Chem. A*, **105**, 7267 (2001).
[15] R.M. Burger, S.B. Horwitz, J. Peisach, J.B. Wittenberg. Oxygenated iron bleomycin—short-lived intermediate in the reaction of ferrous bleomycin with O-2. *J. Biol. Chem.*, **254**, 2299 (1979).
[16] C.C. Cheng, J.G. Goll, G.A. Neyhart, T.W. Welch, P. Singh, H.H. Thorp. Relative rates and potentials of competing redox processes during DNA cleavage–oxidation mechanisms and sequence-specific catalysis of the self-inactivation of oxometal oxidants by DNA. *J. Am. Chem. Soc.*, **117**, 2970 (1995).
[17] M. Nakamura, J. Peisach. Self-inactivation of Fe(II)–bleomycin. *J. Antibiotics*, **41**, 638 (1988).
[18] C.Q. Zhao, C.W. Xia, Q.K. Mao, H. Forsterling, E. DeRose, W.E. Antholine, W.K. Subczynski, D.H. Petering. Structures of HO_2—Co(III)bleomycin A(2) bound to d(GAGCTC)(2) and d(GGAAGCTTCC)(2): structure-reactivity relationships of Co and Fe bleomycins. *J. Inorg. Biochem.*, **91**, 259 (2002).
[19] M. Swart, A.R. Groenhof, A.W. Ehlers, K. Lammertsma. Validation of exchange-correlation functionals for spin states of iron complexes. *J. Phys. Chem. A*, **108**, 5479 (2004).

[20] P.J. Hay, W.R. Wadt. *J. Chem. Phys.*, **82**, 270 (1985).
[21] M.J. Frisch, G.W. Trucks, H.B. Schlegel, G.E. Scuseria, M.A. Robb, J.R. Cheeseman, V.G. Zakrzewski, J.A. Montgomery Jr., R.E. Stratmann, J.C. Burant, S. Dapprich, J.M. Millam, A.D. Daniels, K.N. Kudin, M.C. Strain, Ö. Farkas, J. Tomasi, V. Barone, M. Cossi, R. Cammi, B. Mennucci, C. Pomelli, C. Adamo, S. Clifford, J. Ochterski, G.A. Petersson, P.Y. Ayala, Q. Cui, K. Morokuma, P. Salvador, J.J. Dannenberg, D.K. Malick, A.D. Rabuck, K. Raghavachari, J.B. Foresman, J. Cioslowski, J.V. Ortiz, A.G. Baboul, B.B. Stefanov, G. Liu, A. Liashenko, P. Piskorz, I. Komáromi, R. Gomperts, R.L. Martin, D.J. Fox, T. Keith, M.A. Al-Laham, C.Y. Peng, A. Nanayakkara, M.M.W. Challacombe, P.M.W. Gill, B. Johnson, W. Chen, M.W. Wong, J.L. Andres, C. Gonzalez, M. Head-Gordon, E.S. Replogle, J.A. Pople. *Gaussian03, Revision C.02*, Gaussian Inc., Wallingford, CT (2004).
[22] R. Car, M. Parrinello. Unified approach for molecular-dynamics and density-functional theory. *Phys. Rev. Lett.*, **55**, 2471 (1985).
[23] J. Hutter, A. Alavi, T. Deutsch, M. Bernasconi, S.T. Goedecker, D. Marx, M. Tuckerman, M. Parrinello. CPMD version 3.9, Copyright IBM Corp 1990–2005, Copyright MPI fuer Festkoerperforschung Stuttgart 1997–2001.
[24] N. Troullier, J.L. Martins. Efficient pseudopotentials for plane-wave calculations. *Phys. Rev. B*, **43**, 1993 (1991).
[25] A.D. Becke. Density functional calculations of molecular-bond energies. *J. Chem. Phys.*, **84**, 4524 (1986).
[26] J.P. Perdew. Density-functional approximation for the correlation-energy of the inhomogeneous electron-gas. *Phys. Rev. B*, **33**, 8822 (1986).
[27] A. Laio, J. VandeVondele, U. Rothlisberger. D-RESP: dynamically generated electrostatic potential derived charges from quantum mechanics/molecular mechanics simulations. *J. Phys. Chem. B*, **106**, 7300 (2002).
[28] A. Laio, J. VandeVondele, U. Rothlisberger. A Hamiltonian electrostatic coupling scheme for hybrid Car–Parrinello molecular dynamics simulations. *J. Chem. Phys.*, **116**, 6941 (2002).
[29] W.F. van Gunsteren, S.R. Billeter, A.A. Eising, P.H. Huenenberger, P. Krueger, A.E. Mark, W.R.P. Scott, I.G. Tironi. *Biomolecular Simulation: The Gromos96 Manual and User Guide*, Hochschulverlag an der ETH Zurich, Zurich, Switzerland (1996).
[30] H.J.C. Berendsen, G. Postma, W.F. van Gunsteren, J. Hermans. Interactions models for water in relation to protein hydratation. In *Intermolecular Forces*, B. Pullmann (Ed.), p. 331, Reidel Publishing Company, Dordrecht, The Netherlands (1981).
[31] F. Fedeles, M. Zimmer. Conformational/configurational analysis of all the binding geometries of cobalt(III) bleomycin. *Inorg. Chem.*, **40**, 1557 (2001).
[32] T.E. Lehmann, M.L. Serrano, L. Que. Coordination chemistry of Co(II)-bleomycin: its investigation through NMR and molecular dynamics. *Biochemistry*, **39**, 3886 (2000).
[33] M. Sugiyama, T. Kumagai, M. Hayashida, M. Maruyama, Y. Matoba. The 1.6-A crystal structure of the copper(II)-bound bleomycin complexed with the bleomycin-binding protein from bleomycin-producing *Streptomyces verticillus*. *J. Biol. Chem.*, **277**, 2311 (2002).
[34] A. Karawajczyk, F. Buda. The metal bonding domain of the antitumor drug Fe(II)–bleomycin: a DFT investigation. *J. Biol. Inorg. Chem.*, **10**, 33 (2005).
[35] A. Karawajczyk, C. Gossens, U. Rothlisberger, F. Buda. Mechanism of bleomycin suicide: a Car–Parrinello molecular dynamics investigation. *J. Phys. Chem. B*, **110**, 21245 (2006).